Ferroelectricity and superparamagnetism in Sr/Ti nonstoichiometric SrTiO_{3}

Y. Y. Guo, H. M. Liu, D. P. Yu, and J.-M. Liu

Phys. Rev. B **85**, 104108 — Published 22 March 2012

DOI: 10.1103/PhysRevB.85.104108

Revised Manuscript submitted to Physical Review B: Brief Report (BKJ1146 Guo)

Ferroelectricity and superparamagnetism in Sr/Ti nonstoichiometric $SrTiO_3$

Y. Y. Guo[1], H. M. Liu[1], D. P. Yu[2], and J. –M. Liu[1,3,4]

[1]*Laboratory of Solid State Microstructures, Nanjing University, Nanjing 210093, China*

[2]*Electron Microscopy Laboratory, Peking University, Beijing 100871, China*

[3]*Institute of Advanced Materials, South China Normal University, Guangzhou 510006, China*

[4]*International Center for Materials Physics, Chinese Academy of Sciences, Shenyang, China*

[Abstract] The effect of Sr/Ti nonstoichiometry on the ferroelectricity and magnetism in polycrystalline $SrTiO_3$ is investigated by the dielectric, ferroelectric, Raman, and magnetic characterizations. It revealed that the nonstoichiometric $SrTiO_3$ exhibits both ferroelectric polarization and superparamagnetism which increase with the degree of nonstoichiometry. It is argued that the antisite-like defects with net local dipoles and magnetic moments contribute to the ferroelectricity and superparamagnetism, confirmed by the first-principles calculations.

PACS numbers: 77.84.Cg, 68.55.Ln, 77.80.-e, 75.60.Ej, 71.15.Mb

Keywords: $SrTiO_3$, nonstoichiometry, magnetism, ferroelectricity

Perovskite $SrTiO_3$ (STO) is a well-known quantum paraelectric compound and has been receiving attentions in the past decades.[1-5] Because one of the triply degenerate R_{25} modes is frozen, the cubic STO phase transforms into an antiferrodistortive tetragonal structure below temperature T<105K.[3] Further cooling leads to a rapid increasing of dielectric permittivity (ε) with decreasing T and eventually a T-independent plateau appears below T~4K. Unfortunately, no ferroelectric (FE) transition occurs even though T is down to the lowest limit available.[1-3]

Nevertheless, such a quantum paraelectric state is fragile and an FE instability may occur against even weak intrinsic or external stimulus, which has been a hot topic for intensive focus.[5] For example, the FE instability can be induced by A-site doping,[3,4] oxygen isotope substitution,[2] mechanical stress or external electric field.[6,7] Recent experiments revealed the ferroelectricity in slightly nonstoichiometric STO thin films,[8-11] which represents an alternative approach to modulate the FE instability. It should be mentioned that the physics underlying this nonstoichiometry-induced effect is still under debate and a well acceptable explanation remains open. Since the nonstoichiometric thin films were homoepitaxial on STO single crystal substrates, local lattice distortion inside the films due to the nonstoichiometry could be somehow restricted by the underlying substrate.[8,10,12] A revisit of the intrinsic effect of Sr/Ti nonstoichiometry in bulk STO with no more substrate restriction is necessary.

On the other hand and more attractively, a recent first-principles calculation[11] predicts potential magnetic moment of ~$2\mu_B$ in Ti-rich STO due to the two non-bonded electrons associated with the off-centered Ti interstitial (i.e. Ti^{2+} ion). Besides, this calculation also suggests that the Ti antisite-like defects (Ti_{OC}) deviated from the stoichiometry could be responsible for the ferroelectricity. The local defect pair composed of a negatively charged Sr vacancy (V_{Sr}^{2-}) and positively charged Ti interstitial (Ti^{2+}) constitutes a Ti^{2+}-V_{Sr}^{2-} electric dipole, and those dipoles in order contribute to polarization P. This suggests the concurrence of magnetism with ferroelectricity in nonstoichiometric STO, at least in Ti-rich STO, while the stoichiometric bulk STO itself should be diamagnetic[13] and is believed to be free of both FE and spin orders.[14,15] In this work, we address the magnetism and ferroelectricity in polycrystalline STO by synthesizing a set of Ti-rich and Sr-rich samples and characterizing their dielectric, ferroelectric, Raman, and magnetic behaviors. In parallel, the first-principles calculation based on the VASP package is also performed to further clarify the proposed Ti

antisite-like defects mechanism and extend it to both the Ti-rich and Sr-rich cases.

In fact, it is difficult to synthesize high quality nonstoichiometric STO samples by conventional solid-state reaction route. In this work, high quality polycrystalline STO samples with different Sr/Ti ratios (x) (x=0.85~1.15) were prepared by the two-step molten salt method.[16] The advantages of this method include the relatively high precision composition control with respect to the nominal composition, and very low density of oxygen vacancies (if not free) other than those vacancies controlled by the electric neutrality.

In our experiment, highly purified $SrCO_3$, TiO_2, and NaCl powder was mixed, ground, and calcined at 880ºC for 7h in air. The products were washed repeatedly with hot deionized water to remove NaCl. Additional NaCl powder was then added to the resultant products, and the mixtures were calcined again at 950ºC for 10h in air. The fully washed powders were pressed under 20MPa into disks of 20mm diameter and 1.5mm thickness, and then sintered at 1150°C for 20h in air. It is addressed that these samples were prepared with the identical procedure, and the careful chemical composition analysis of them using the energy dispersive X-ray spectrometry was made. The measured x values fit well the nominal compositions within the ±0.5% measuring uncertainties.

The microstructures including the grain size were characterized by scanning electron microscopy (SEM). The crystallinity of the as-prepared samples was checked by X-ray diffraction (XRD) with Cu $K\alpha$ radiation at room temperature. Gold electrodes were sputtered on the sample surfaces for electric measurements. The ε data were measured using HP4294A impedance analyzer in connection with the Quantum Design physical property measurement system (PPMS). For measuring polarization P, we employed the pyroelectric current method with an electrometer (Keithley 6514) under a pre-poling electric field E=14kV/cm, and details of the procedure can be referred to earlier literature.[14] To check the FE instability, the Raman spectroscopy was undertaken using a Renishaw inVia Raman microscope with an Ar ion laser (514nm) source (Sterllar-REN 514-50). The spectra were recorded in the backscattering geometry over the T-range from 10K to 350K. The magnetic measurements were performed using the superconducting quantum interference device (SQUID) magnetometer under the zero-field-cooled (ZFC) and field-cooling (FC) modes with a measuring field H=1kOe.

Surely, a drawback of polycrystalline sample is the possible grain boundary effect. In our

experiment, we optimized the synthesis procedure to obtain the high-density samples. The average grain size (mean intercept length on the fracture surface, measured by SEM) is almost same for all as-prepared STO samples, as shown in Fig.1. Thus, grain boundaries effects, if any, should contribute to various measured properties in the same or nearly the same way, approximately independently of the stoichiometry. Consequently, we can argue that the evaluated data have sufficient physical significance.

To confirm the sample crystallinity, we present the XRD data in Fig.2(a) for several samples. It is seen that as the off-stoichiometry reaches a higher value, the small amount of secondary phases will appear. In fact, when the excess Sr reaches a higher value, the Ruddlesden-Popper (RP) ($SrO\cdot(SrTiO_3)_n$) phase will be present. Fig.2(a) shows that secondary phases TiO_2 and RP appear in Ti-rich (x=0.85) and Sr-rich (x=1.15) STO samples, respectively. In comparison, all of those samples with smaller off-stoichiometry ($0.93\leq x\leq 1.10$) exhibit a single perovskite structure and the TiO_2 and RP phases could not be observed within the apparatus resolution. Thus, we can argue that the TiO_2 and RP phases in Ti-rich and Sr-rich STO samples with small off-stoichiometry values ($0.93\leq x\leq 1.10$) are all very tiny or hardly detectable. In our work, we study the ferroelectricity and magnetism of those samples with small off-stoichiometry STO samples ($0.93\leq x\leq 1.10$).

Table I lists the lattice parameters and volume for STO samples obtained from their x-rays data. One can see from the table that the lattice gradually expands along a, b and c directions with the degree of nonstoichiometry, no matter whether in Ti-rich or Sr-rich case. The resultant increase in volume is also observed. However, those previous studies on homoepitaxial nonstoichiometric STO films only reported the increase of the out-of-plane film lattice parameter (c) due to the non-relaxed compressive biaxial strain from the underlying substrate. These changes suggest that in homoepitaxial nonstoichiometric STO films, local lattice distortions inside the films due to the nonstoichiometry can be only partially relaxed. Therefore, one can more clearly and intuitively study the intrinsic effect of nonstoichiometry on the ferroelectricity in bulk STO without the substrate restriction.

To illustrate the significance of the pyroelectric current method for FE polarization, we present in Fig.2(b) the data for sample x=0.96 as a typical example. The sample is first cooled down to T=2K under an electric field (E=14kV/cm, and the direction of E perpendicular to the

disk-like sample surface), and then the T-dependence of pyroelectric current I is measured after a sufficiently long time (t) short-circuit procedure. To check the contribution of possible trapped charge release to the measured current, we collect the data at three different warming ramp rates (2, 4, and 6K/min). It is seen that the peak of the I–T curve does not shift along the T-axis, and the evaluated areas below the curves divided respectively by the ramp rates are the same. This indicates that no contribution from possible trapped charge release is available and the pyroelectric current is dominant. The polarization P, integrated from the $I(t)$, is shown in Fig.2(c). Therefore, we demonstrate that this nonstoichiometric STO sample does exhibit ferroelectricity at low T although the polarization is not big.

Fig.3(a) and (b) show the measured $\varepsilon(T)$ for a series of samples. It is noted that the degree of nonstoichiometry (DONS) from both sides (i.e. the deviation of x from 1.00) leads to the appearance of a broad dielectric peak at low T, which shifts gradually towards the high-T side with increasing DONS. The dielectric peak at $T=T_m$ features the FE transition. The gradually enhanced P with DONS from both sides is identified in Fig.3(c), although a tiny P is recorded for sample x~1.00. A possible reason for the small ferroelectricity of sample x~1.00 is the tiny nonstoichiometry, because it is experimentally difficult to strictly control the Sr/Ti ratio to be ONE. The similar phenomenon was also observed in nominally stoichiometric STO single crystals and epitaxial films, arising from minute amounts of nonstoichiometry.[9] Probably the grain boundaries in polycrystalline samples also contribute weakly to the ferroelectricity. Particularly, in our work, we employed the pyroelectric current method for measuring polarization P. This method is very accurate, and its precision can reach up to 10^{-15}A. Under this high precision, it is reasonable to measure such signal even in nominally stoichiometric polycrystalline sample. Here we would like to mention that stoichiometric STO was reported to exhibit weak ferroelectricity under a strong electric field,[6] which is reasonable considering STO itself is close to the ferroelectric instability. However, in our pyroelectric current method, no electric field is applied to the sample during the measurement. Taking the $P(T)$ data from the nominal STO sample (x~1.00) as a reference, one can conclude that the emerging polarization for the other samples should come from the Sr/Ti nonstoichiometry.

As shown in the inset of Fig.3(c), the evaluated $P(x)$ at T=4K and $T_m(x)$, both of which are V-shaped, indicate clearly the nonstoichiometry induced ferroelectricity. In addition, the

induced FE state shows weak relaxor behavior, evidenced by the broad dielectric peaks and weak dielectric dispersions given in the insets of Fig.3(a) and (b) for two samples, respectively. To this stage, the presented data do confirm the nonstoichiometry generated ferroelectricity in STO, a remarkable effect.

We also provide the Raman spectroscopy evidence on the FE instability, as shown in Fig.4, while the data below 200cm^{-1} are not available for our apparatus. The Raman spectrum at 10K for sample x~1.00 is characterized by the broad second-order scattering signal and structural mode R (Fig.4(a)). The first-order Raman scattering peaks arising from the polar modes (LO_3, TO_4, and LO_4 modes) are also visible but quite weak, probably due to the tiny nonstoichiometry and polycrystalline nature. In fact, the appearance of the strong LO_3, TO_4, and LO_4 phonon peaks can be taken as an indicator of the paraferroelectric transition.[9] For the other samples, these polar peaks become significant and their intensities increase with increasing DONS. The T-dependent Raman spectra of samples x~0.93 and 1.10 (Fig.4(b) and (c)) clearly show the considerable first-order peaks at low T which emerge gradually with decreasing T, indicating that the related modes become Raman-active due to the symmetry selection rules associated with the ferroelectricity generation.

Now we turn to the magnetism of these samples. As a reference, the magnetization M of a commercial STO single crystal was measured too. For the sake of clarity, we present in Fig.5 the measured M-T and M-H data for a series of samples. While all the samples exhibit the diamagnetic behavior in the high T-range, the clear positive magnetization at low T is identified for the nonstoichiometric samples. We focus on the measured M-H loops at T=4K, as shown in Fig.5(b). Recent first-principle study[11] suggests that each off-centered interstitial Ti^{2+} deviated from the stoichiometry can introduce a magnetic moment of ~2μ_B. However, given no existence of the long-range correlations between these moments in the as-prepared samples, a ferromagnetic long range order seems unavailable. Here we would describe this low-T magnetism as superparamagnetic behavior in view of several features. First, an S-shaped M-H curve is observed, as it appears with almost zero remnant magnetization and coercive field. Second, no saturation of M at high H can be reached while the moment is relatively small (for sample x~0.93, M~0.03emu/g at H=20kOe). Third, nearly no difference in the M-T curves between the ZFC mode and FC one is observed. In spite of this

super-paramagnetism, one finds the bigger magnetic moment the larger the DONS, indicating the stronger spin correlation tendency in more nonstoichiometric sample.

The XRD data in Fig.2 already identify that the possible impurities in Ti-rich and Sr-rich STO samples ($0.93 \leq x \leq 1.10$), even if any, are very tiny or scarcely detectable TiO_2 and RP phases, respectively. According to magnetism theory, TiO_2 and RP phases are presumably diamagnetic and do not contribute to the paramagnetic response, because neither Ti^{4+}/Sr^{2+} nor O^{2-} are magnetic ions and the *d*-shells of these cations are empty.[13,17] Thus, the low *T* superparamagnetism could be mainly attributed to the formation of antisite-like defects.

To further clarify the Ti antisite-like defects mechanism proposed in the recent first-principles study[11] and extend it to both the Ti-rich and Sr-rich cases, we perform extensive first-principles calculations. The calculation is performed using the Vienna *ab-initio* simulation package (VASP) code[18] and the Perdew-Becke-Erzenhof (PBE) generalized gradient approximation (GGA) function.[19] The projector augmented wave (PAW) pseudopotential[20] is utilized with a plane wave energy cutoff at 500eV. In order to correct the on-site Coulomb interaction, a rotationally invariant Density Functional Theory (DFT)+*U*[21] method on the *d*-orbital of the Ti^{4+} ion (U=5.0eV) is used, and the Hund rule coupling factor J_H=0.64eV is fixed during the entire calculations. It should be mentioned here that the first-principles approach to the slight nonstoichiometric system can be tough since the required cell size can be extremely large, challenging the current calculation. Without losing the generality, we choose the lattices of Sr/Ti=7/9 and Sr/Ti=9/7, i.e. x~0.78 and x~1.28 as examples for a qualitative illustration. The unit cells chosen for Ti-rich lattice are the same as those in literature.[11] The similar scenario applies to the Sr-rich lattice with Sr antisite-like defects (Sr_{OC}), where the negatively charged Ti vacancies (V_{Ti}^{4-}) and positively charged Sr interstitials (Sr^{4+}) constitute the Sr^{4+}-V_{Ti}^{4-} electric dipoles in order and may contribute to the superparamagnetism and electric polarization in Sr-rich STO.

For sample x~0.78, the total moment of ~$2\mu_B$ is confirmed by our calculations. The electronic band structure is depicted in Fig.6(a). The density of state (DOS) at the Fermi level is zero, thus this sample is an insulator. Moreover, the densities of localized one-electron states in the majority (red line) and minority (blue line) spin components are non-symmetric, yielding a spin polarization with moments of ~$2\mu_B$, due to the two non-bonded 3d electrons

associated with the off-centered Ti interstitial (i.e. Ti^{2+} ion). Given the knowledge on the magnetism and band structure, we evaluate the FE polarization using the Berry phase method.[22] The predicted P value for x~0.78 is ~1.3C/m^2, conclusively confirming the ferroelectricity, noting that no sample with x~0.78 can be synthesized by conventional route for a quantitative comparison. For sample x~1.28, the calculated magnetic moment is ~2μ_B too, due to the four 4p electrons associated with the off-centered Sr interstitial (i.e. Sr^{4+} ion). But unfortunately this sample is a half-metal as derived from the band structure, and thus no polarization can be given.

If one goes further for a quantitative comparison, the predicted P value and magnetic moment are both much bigger than the measured ones here. In fact, the large difference between calculated and experimental values of ferroelectric polarization P seems common for quite a number of magnetic ferroelectric oxides.[23] The disagreement in P may be caused by several factors. First, in first principle calculations, the employed models are anyway much simpler than real materials and the calculations grasp the main physics, but a quantitative consistency refers only to few cases. Moreover, the periodic boundary conditions in first principle calculations mean that the off-centered antisite-like defects are in an ordered arrangement. However, in real materials, these antisite-like defects arrangement may be random or in disorder to a great extent, giving a much smaller measured P than the calculated one. In addition, considering the calculation amount, the samples used for the calculations are more seriously nonstoichiometric than the synthesized ones, contributing a relatively big calculated P. Another reason for the difference in P is that in our work, the materials are polycrystalline samples while we simulate single crystal models in first principle calculations. For magnetic ferroelectric oxides such as multiferroic manganites, the polarization measured in polycrystalline samples is usually one order of magnitude smaller than the single crystal sample.

The difference between the measured M (~0.048μ_B per defect) and calculated one (~2μ_B per defect) could be attributed to oxygen vacancies which are inevitable during the sample preparation. In both the Ti-rich (x~0.78) and Sr-rich (x~1.28) cases, our calculations show no net magnetic moment if one oxygen vacancy is allowed in accompanying with one antisite-like defect, in agreement with previous work.[11] In the other words, oxygen vacancies

seem to seriously suppress the magnetic moment, which can be a major reason for the much smaller measured M than the calculated one. Other possible reasons for the quantitative disagreement between calculated and experimental values of P and M remain open, and additional ingredient of physics and other possible mechanisms may be taken into account.

In conclusion, a series of Ti-rich or Sr-rich bulk STO samples were synthesized and the effects of nonstoichiometry on the ferroelectricity and magnetism have been investigated. The dielectric, polarization, Raman, and magnetism measurement results indicate that the ferroelectric and super-paramagnetic responses gradually strengthen with the degree of off-stoichiometry. The antisite-like defects with a net local dipole and magnetic moment are suggested to be responsible for these phenomena.

Acknowledgement:

This work was supported by the Natural Science Foundation of China (11074113, 50832002), the National 973 Projects of China (2011CB922101, 2009CB623303), the Natural Science Foundation of Jiangsu Province, China (BK2008024), and the Priority Academic Program Development of Jiangsu Higher Education Institutions, China.

References:

1. J. G. Bednorz and K. A. Müller, Phys. Rev. Lett 52, 2289 (1984).
2. M. Itoh, R. Wang, Y. Inaguma, T. Yamaguchi, Y.-J. Shan, and T. Nakamura, Phys. Rev. Lett. 82, 3540 (1999).
3. G. Geneste and J.-M. Kiat, Phys. Rev. B 77, 174101 (2008).
4. A. Tkach, P. M. Vilarinho, and A. L. Kholkin, Appl. Phys. Lett. 86, 172902 (2005).
5. S. E. Rowley, L. J. Spalek, R. P. Smith, M. P. M. Dean, G. G. Lonzarich, J. F. Scott, and S. S. Saxena, arXiv: 0903.1445 (2009).
6. P. A. Fleury and J. M. Worlock, Phys. Rev. 174, 613 (1968).
7. J. H. Haeni, P. Irvin, W. Chang, R. Uecker, P. Reiche, Y. L. Li, S. Choudhury, W. Tian, M. E. Hawley, B. Craigo, A. K. Tagantsev, X. Q. Pan, S. K. Streiffer, L. Q. Chen, S. W. Kirchoefer, J. Levy, and D. G. Schlom, Nature (London) 430, 758 (2004).
8. Y. S. Kim, D. J. Kim, T. H. Kim, T. W. Noh, J. S. Choi, B. H. Park, and J.-G. Yoon, Appl. Phys. Lett. 91, 042908 (2007).
9. H. W. Jang, A. Kumar, S. Denev, M. D. Biegalski, P. Maksymovych, C. W. Bark, C. T. Nelson, C. M. Folkman, S. H. Baek, N. Balke, C. M. Brooks, D. A. Tenne, D. G. Schlom, L. Q. Chen, X. Q. Pan, S. V. Kalinin, V. Gopalan, and C. B. Eom, Phys. Rev. Lett. 104, 197601 (2010).
10. D. J. Keeble, S. Wicklein, R. Dittmann, L. Ravelli, R. A. Mackie, and W. Egger, Phys. Rev. Lett. 105, 226102 (2010).
11. M. Choi, F. Oba, and I. Tanaka, Phys. Rev. Lett. 103, 185502 (2009).
12. E. J. Tarsa, E. A. Hachfeld, F. T. Quinlan, J. S. Speck, and M. Eddy, Appl. Phys. Lett. 68, 490 (1996).
13. M. Khalid, A. Setzer, M. Ziese, P. Esquinazi, D. Spemann, A. Poppl, and E. Goering, Phys. Rev. B 81, 214414 (2010).
14. T. Kimura, T. Goto, H. Shintani, K. Ishizaka, T. Arima, and Y. Tokura, Nature (London) 426, 55 (2003).
15. K. F. Wang, J. –M. Liu, and Z. F. Ren, Adv. Phys. 58, 321 (2009).
16. K. Watari, B. Brahmaroutu, G. L. Messing, and S. Trolier-McKinstry, J. Mater. Res. 15

846 (2000).

17. M. Venkatesan, C. B. Fitzgerald, and J. M. D. Coey, Nature (London) 430, 630 (2004).
18. G. Kresse and J. Furthmüller, Phys. Rev. B 54, 11169 (1996).
19. J. P. Perdew, K. Burke, and M. Ernzerhof, Phys. Rev. Lett. 77, 3865 (1996).
20. P. E. Blöchl, Phys. Rev. B 50, 17953 (1994); G. Kresse and D. Joubert, Phys. Rev. B 59, 1758 (1999).
21. A. I. Liechtenstein, V. I. Anisimov, and J. Zaanen, Phys. Rev. B 52, 5467 (1995).
22. R. D. King-Smith and D. Vanderbilt, Phys. Rev. B 47, 1651(1993).
23. E. Bousquet, N. A. Spaldin, and P. Ghosez, Phys. Rev. Lett. 104, 037601 (2010).

Captions for figures:

Fig.1. Scanning electron microscopy (SEM) images of the fracture surfaces of several samples (x=0.93~1.10).

Fig.2. (Color online) (a) X-ray diffraction patterns for several samples (x=0.85~1.15). (b) Measured pyroelectric current data $I(T)$ at three different warming ramp rates (2, 4, and 6K/min) for sample x=0.96. (c) T-dependence of P for sample x=0.96.

Fig.3. (Color online) Measured T-dependence of ε at frequency of 1.0 kHz for (a) Sr-rich STO samples and (b) Ti-rich STO samples. (c) Measured polarization $P(T)$ data for several samples. Insets: $\varepsilon(T)$ data at different frequencies (0.1 kHz, 1.0 kHz, 10 kHz, and 100 kHz) for (a) x~1.10 and (b) x~0.93. (c) Evaluated $T_m(x)$ and $P(x)$ at T=4K.

Fig.4. (Color online) (a) Raman spectra for several samples at T=10K. The T-dependent spectra for (b) x~0.93 and (c) x~1.10. The vertical dashed lines are guides for eye showing the first-order phonon peaks.

Fig.5. (Color online) (a) Measured M-T relations for samples x~0.96, 1.00, 1.03, and STO single crystal. (b) M-H hysteresis loops for several samples at T=4K. The inset shows the M-T curves under ZFC and FC conditions for sample x=0.96.

Fig.6. (Color online) Calculated electronic band structures for (a) x~0.78 and (b) x~1.28, without considering oxygen vacancies.

Table I. Lattice parameters and volume for STO samples with different Sr/Ti ratios (x) (x=0.93~1.10) obtained from the X-ray diffraction data.

x	0.93	0.96	1.00	1.03	1.06	1.10
a (Å)	3.90998	3.90837	3.90409	3.90413	3.90554	3.90897
b (Å)	3.91144	3.90906	3.90416	3.90456	3.90706	3.91014
c (Å)	3.91198	3.90984	3.90419	3.90492	3.90751	3.91084
V(Å^3)	59.82842	59.73482	59.50841	59.5262	59.62516	59.77515

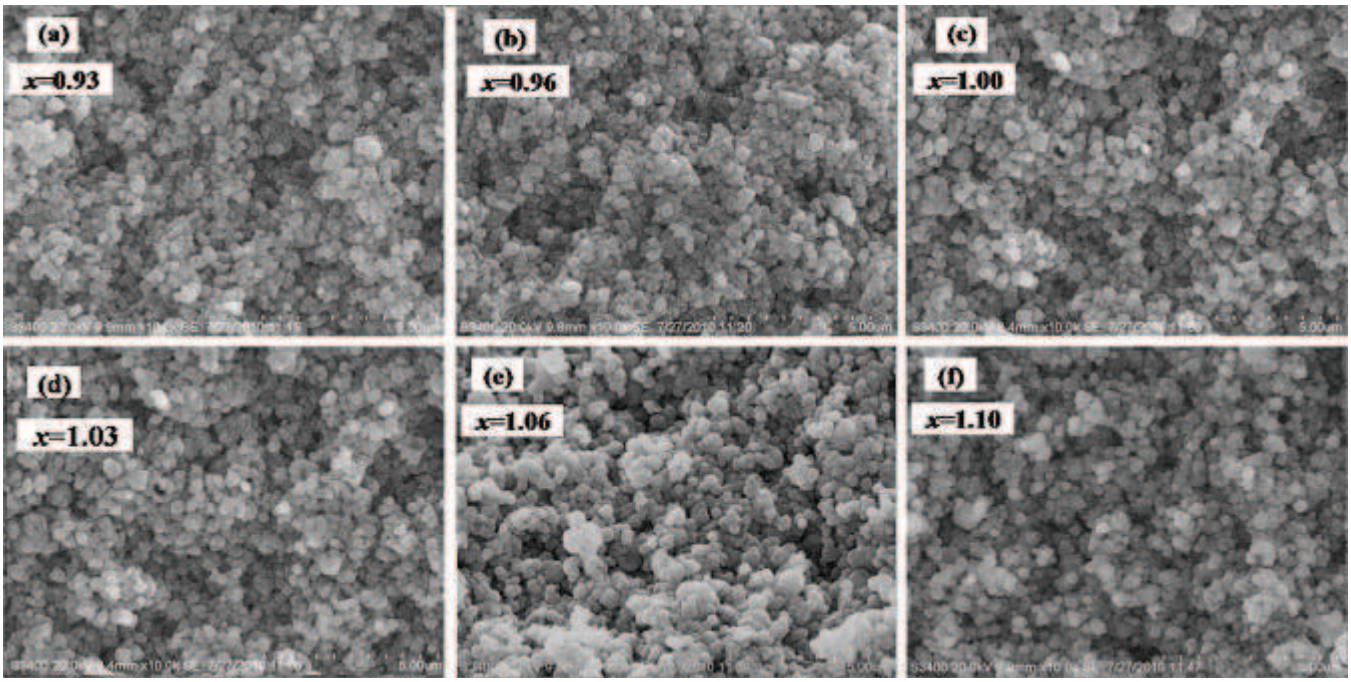

Figure 1 BKJ1146 06FEB2012

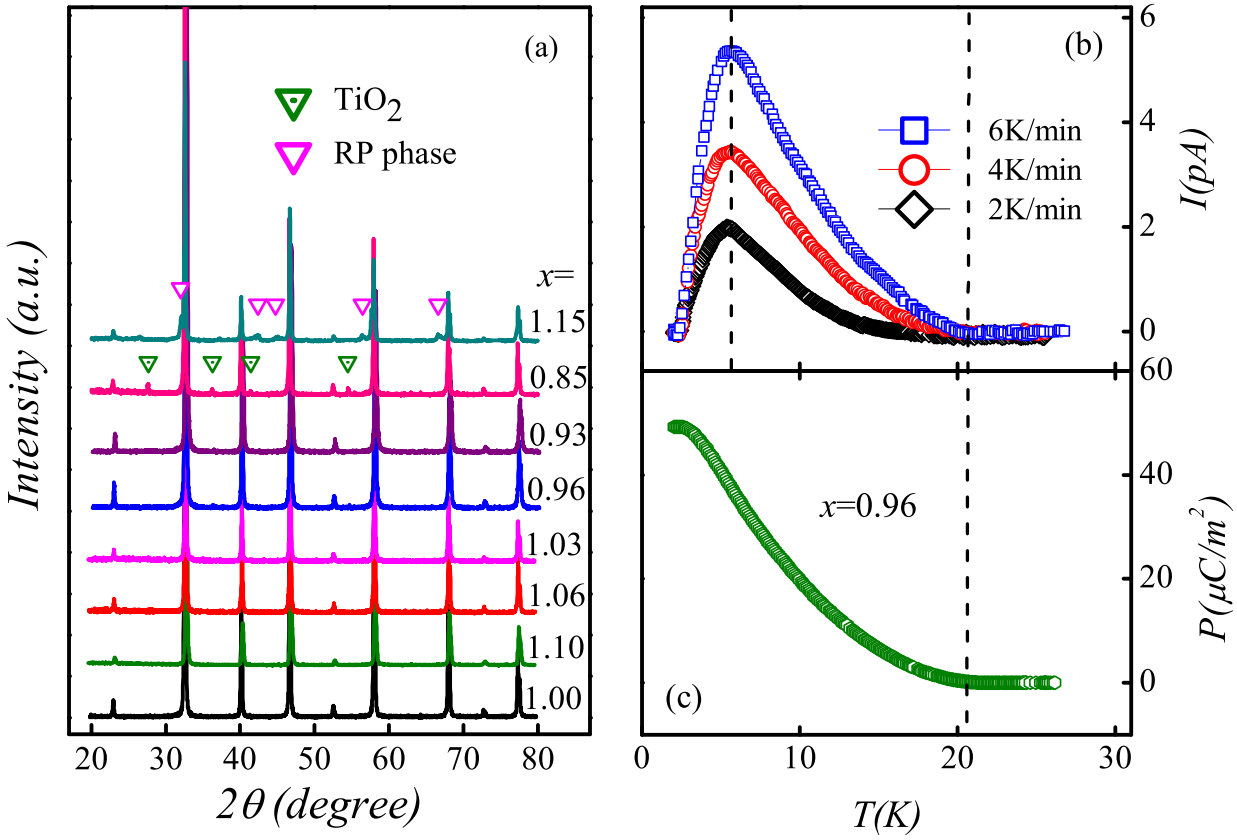

Figure 2 BKJ1146 06FEB2012

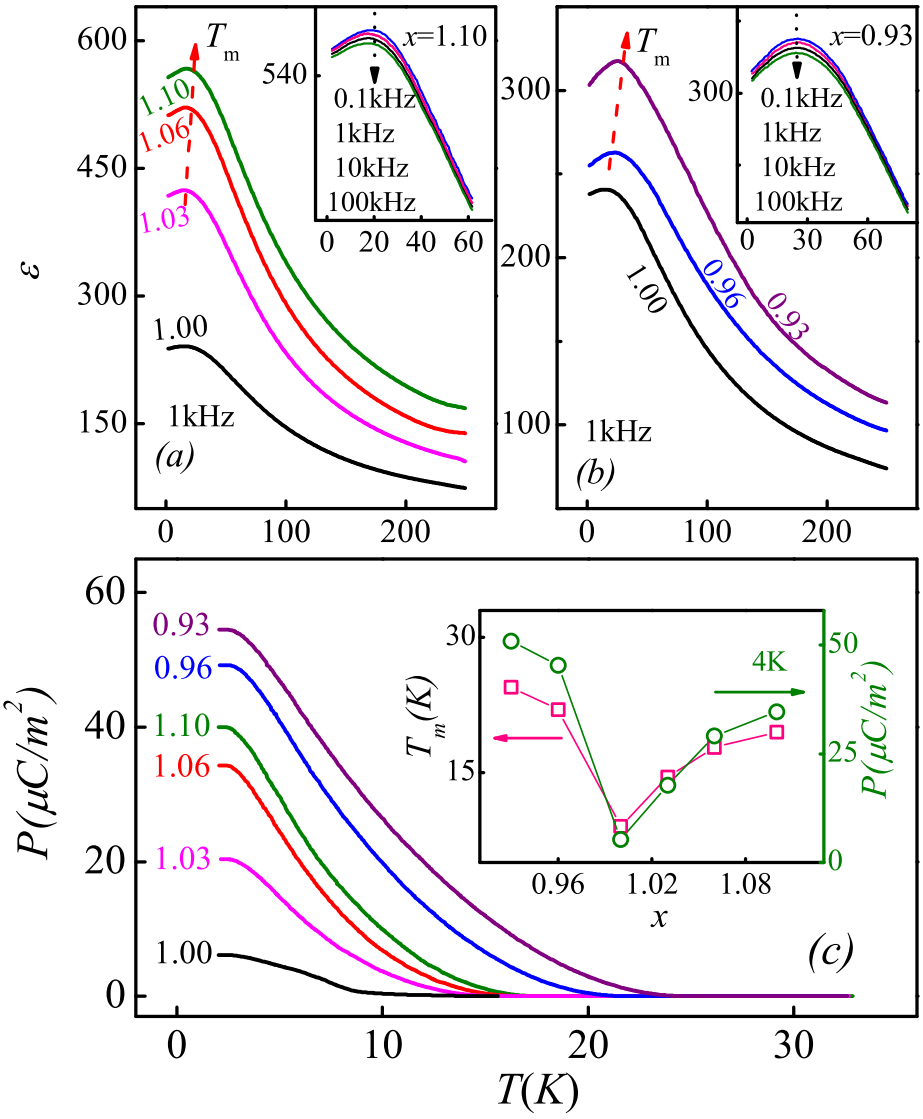

Figure 3 BKJ1146 06FEB2012

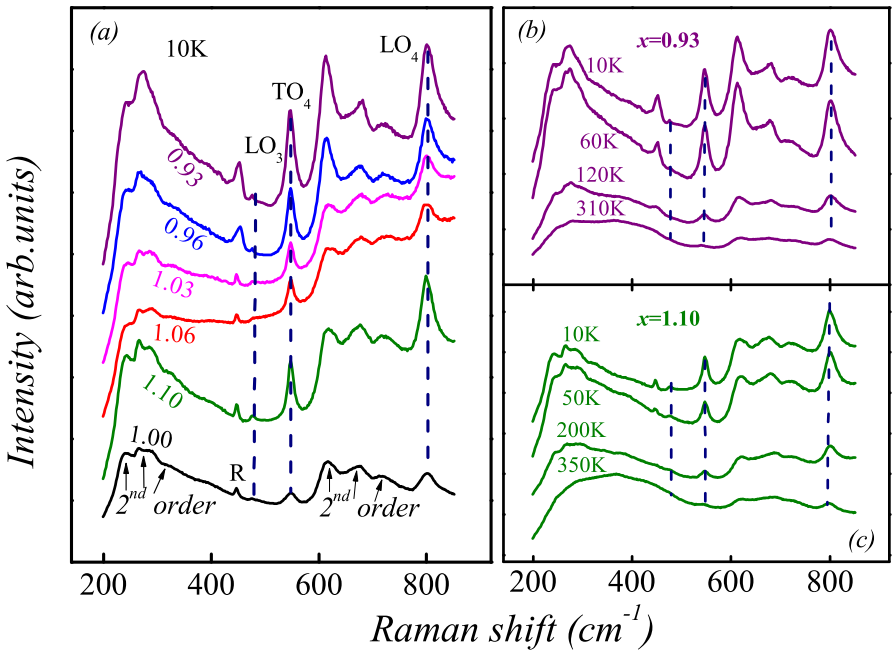

Figure 4 BKJ1146 06FEB2012

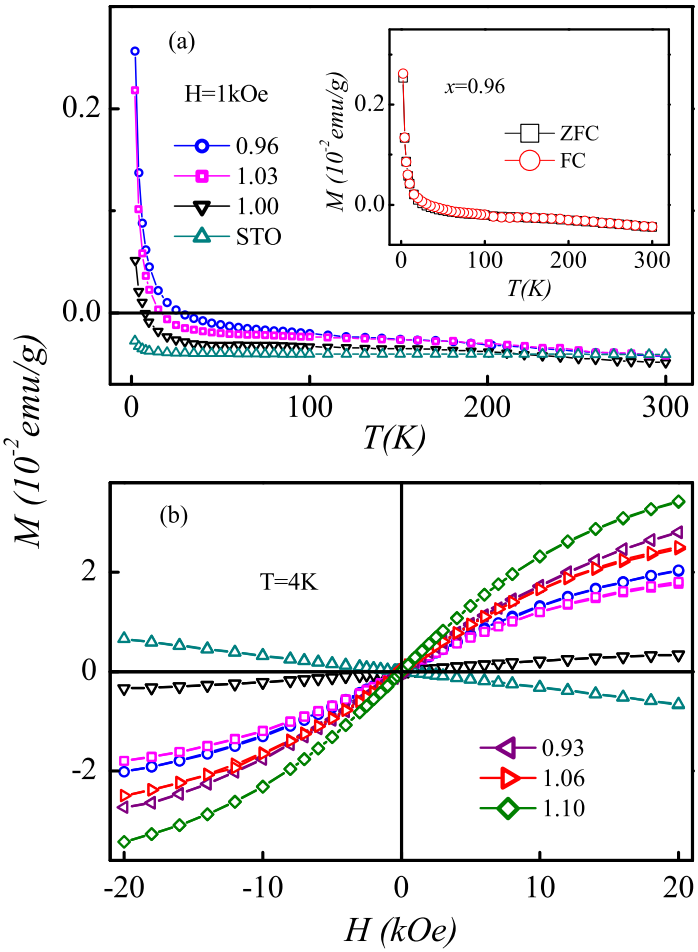

Figure 5 BKJ1146 06FEB2012

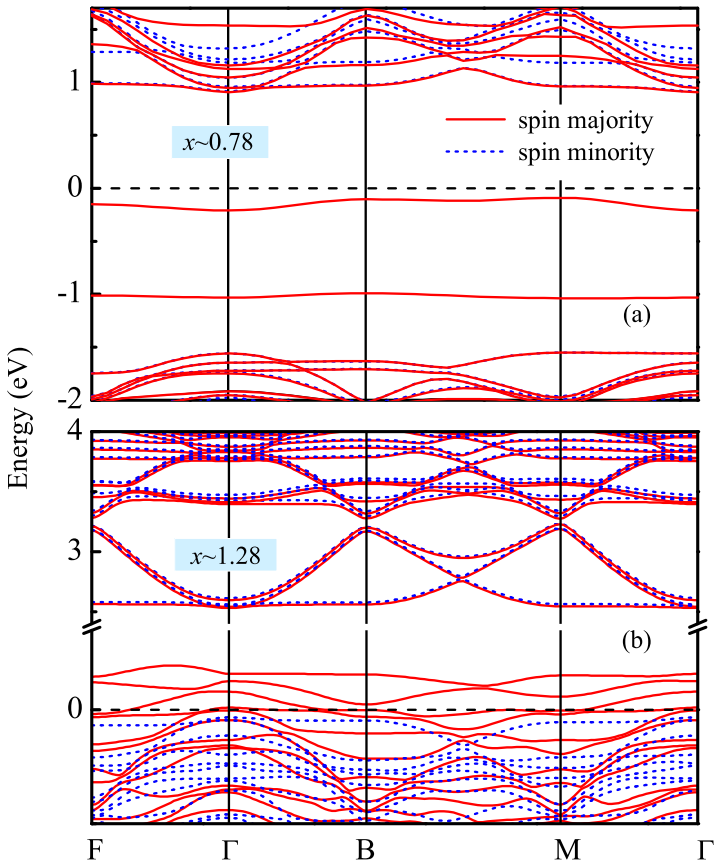

Figure 6 BKJ1146 06FEB2012